Interface focus

J. R. Soc. Interface (2009) **6**, S269–S277
doi:10.1098/rsif.2008.0428.focus
Published online 25 February 2009

Time-lapse observation of cell alignment on nanogrooved patterns

Satoshi Fujita[1,2], Masahiro Ohshima[3] and Hiroo Iwata[1,*]

[1]*Department of Reparative Materials, Institute for Frontier Medical Sciences, Kyoto University, 53 Kawahara-cho, Shogoin, Sakyo-ku, Kyoto 606-8507, Japan*
[2]*Regenerative Medicine Research Center, Itabashi Chuo Medical Center, 2-17-18 Azusawa, Itabashi-ku, 174-0051 Tokyo, Japan*
[3]*Department of Chemical Engineering, Kyoto University, Katsura Campus, Nishikyo-ku, Kyoto 615-8510, Japan*

Cells elongate on a surface with nanogrooved (NG) patterns and align along that pattern. Although various models have been proposed for how this occurs, much remains to be clarified. Studies with fixed cells do not lend themselves to answering some of these open questions. In this study, the dynamic behaviours of living mesenchymal stem cells on an NG substrate with a 200 nm groove depth, an 870 nm ridge width and a 670 nm groove width were observed using time-lapse microscopes. We found that filopodia moved as if they were probing the surroundings of the cell protrusion, and then some cell protrusions invaded the probed areas. Cell protrusions that extended perpendicular to the NG direction tended to retract more rapidly than those parallel to the grooves. From these facts, we think that the retracting phase of cell protrusions play a rule in cell alignment along the NG patterns.

Keywords: contact guidance; filopodia; nanotopography; hot embossing; supercritical CO_2-assisted embossing; mesenchymal stem cell

1. INTRODUCTION

A large number of studies have examined the effects on cell behaviours of surface characteristics, such as wettability, electrostatic charges and functional groups (Witt *et al.* 2004; Navarro *et al.* 2006). These studies form the basis for the development of materials for artificial organs, disposable medical devices and cell culture substrates. In the last decade, the effects of surface micro- and nanotextures on cell adhesion and cell morphology have attracted much attention (Clark *et al.* 1990; Curtis & Wilkinson 1997; Flemming *et al.* 1999; Teixeira *et al.* 2006; Lim & Donahue 2007). Substrates with fine grooves induce various cell responses, such as cell alignment and migration along the grooves (Dalton *et al.* 2001; Diehl *et al.* 2005; Su *et al.* 2007), and, moreover, differentiation of stem cells (Charest *et al.* 2007). Most researchers have assessed cell alignments after cells have been fixed in formaldehyde, methanol or glutaraldehyde. Although those static observations are useful for visualizing intracellular protein fibre alignment in detail, they provide scarce information about dynamic cell behaviours on surfaces with nanopatterns. Studies are needed on dynamic cell behaviours in an acute phase and are expected to give more detailed information on the mechanism of cell alignment on nanogrooved (NG) patterns.

Epithelial cells and fibroblasts have been used to examine cell responses to substrate topography (Lim & Donahue 2007). In this study, we used mesenchymal stem cells (MSCs). MSCs are multipotent stem cells that can differentiate into osteoblasts, adipocytes, chondrocytes and other kinds of mesenchymal cells (Pittenger *et al.* 1999). It has been reported that the morphology of MSCs can determine their fates, such as proliferation or differentiation direction (McBeath *et al.* 2004; Engler *et al.* 2006). In addition, the morphology of MSCs is affected by some physicochemical properties and topography of cell culture substrates (Park *et al.* 2004; Zhu *et al.* 2005; Kurpinski *et al.* 2006; Dalby *et al.* 2007). Thus, we expected that the differentiation direction of MSCs can be controlled by the nanostructure of a substrate. It is meaningful to study the effect of topography of cell culture substrates on the morphology of MSCs.

In this research, NG patterns were printed on polycarbonate (PC) plates using supercritical CO_2-assisted embossing, as previously reported (Fujita *et al.* 2008), and the dynamic behaviours of MSCs on NG patterns were observed under 5 per cent CO_2 and at 37°C using time-lapse microscopes. Time dependence of cell alignment, cell protrusion movements and their remodelling were analysed to infer the mechanism of the topographical effect of the substrate on cell responses.

*Author for correspondence (iwata@frontier.kyoto-u.ac.jp).

Electronic supplementary material is available at http://dx.doi.org/10.1098/rsif.2008.0428.focus or via http://rsif.royalsocietypublishing.org.

One contribution of 10 to a Theme Supplement 'Japanese biomaterials'.

Received 30 August 2008
Accepted 6 January 2009

2. MATERIAL AND METHODS

2.1. Fabrication of the nanogrooved substrate

An NG pattern (200 nm groove depth, 870 nm ridge width and 670 nm groove width; scheme 1*a*) was printed on PC plates using a supercritical CO_2-assisted embossing machine, as reported previously (Fujita *et al.* 2008). In brief, the vessel of the embossing machine was separated into two chambers by a partition. An under pedestal could move between the two chambers through a partition, as a syringe. A disc-shaped PC plate (diameter = 20 mm; thickness = 3 mm; bisphenol-A type; Mw = 58 000; $Tg = 153$°C; Tsutsunaka Plastic Industry Co. Ltd., Osaka, Japan) was placed on top of the pedestal. A nickel mould (supplied by Hitachi Maxell, Ltd., Tokyo, Japan) was set on the ceiling of the upper chamber.

The mould and the PC plate were cleaned by spraying with fluorocarbon gas. The upper chamber was filled with CO_2 gas to 10 MPa, and the chamber temperature was increased to 100°C to achieve the CO_2 supercritical condition. The surface of the PC plate was plasticized by dissolution of CO_2 under the supercritical condition for 5 min. Then, CO_2 was released from the upper chamber, and immediately the pressure of the lower chamber was increased by the introduction of the CO_2 gas to lift the pedestal. The PC plate was pressed to the nickel mould at 12 000–15 000 N for 30 s at 100°C. After stamping, CO_2 was completely released from both chambers and the plate was detached from the mould.

2.2. Cell culture

Human bone marrow-derived MSCs (Lonza, Basel, Switzerland) were maintained in Dulbecco's modified essential medium (DMEM; Invitrogen Corp., Carlsbad, CA, USA) supplemented with 10 per cent foetal bovine serum (FBS; BIOWEST, France), 100 U ml^{-1} penicillin and 100 µg ml^{-1} streptomycin (Invitrogen) at 37°C under 5 per cent CO_2 in a humidified atmosphere, and subcultured at 5×10^3 cells per cm^2 every 3–4 days. Cells at passages 3–8 were used for experiments.

To give cell adherent property to PC plates, they were treated with 10 µg ml^{-1} of fibronectin (Invitrogen) for 2 hours at 37°C (Keselowsky *et al.* 2004), and washed five times with Dulbecco's phosphate-buffered saline Ca^{2+} Mg^{2+} free (DPBS(−); Nissui Pharmaceutical Co. Ltd., Tokyo, Japan). Prior to cell seeding on the fibronectin-coated plates, uniformity of fibronectin coating was examined by immunostaining (electronic supplementary material, figure 1*b*). MSCs were treated with 10 µg ml^{-1} mitomycin C (Wako Pure Chemical Industries, Ltd., Osaka, Japan) for 2 hours to stop cell division, because it is hard to see cell morphology when cell division occurs during a long-term tracking. After the mitomycin C treatment, cells were washed thrice with DPBS(−). The MSCs were seeded at 5×10^3 cells per cm^2 on fibronectin-coated plates and cultured for 4 days in the maintaining medium (DMEM/10% FBS).

2.3. Time-lapse video microscopy

For time-lapse imaging, 1.5×10^4 cells of MSCs, which were treated with 10 µg ml^{-1} mitomycin C and suspended in 300 µl of medium, were seeded onto a fibronectin-treated plate, placed in a 35 mm culture dish and then statically incubated at 37°C under 5 per cent CO_2 for 60 min for adhesion. Then, after the addition of 2 ml medium, the dish was stored in a gas-tight container with capnophilic powder, which consists mainly of ascorbic acid (CulturePal; Corefront Corp., Tokyo, Japan), to maintain 5 per cent CO_2 during observation. For an analysis of cell orientation, cell images were captured every 2.5 min for 5 days using an inverted-phase contrast microscope (Cellwatcher; Corefront).

For visualization of cells under high magnification, a plate carrying MSCs was placed upside down with cells facing a culture dish on a silicone spacer (thickness, 0.5 mm). Cells could be observed under high magnification with an inverted microscope (Biostation IM; Nikon Corp., Tokyo, Japan). For visualization of the extension of cell protrusions, cell images were recorded every 2.5 min for 7 hours. For investigating filopodial movements, time-lapse images were captured every 4 s for 2 hours. Captured images were stacked by ImageJ (v. 1.39f, distributed by NIH) and converted to windows media video format.

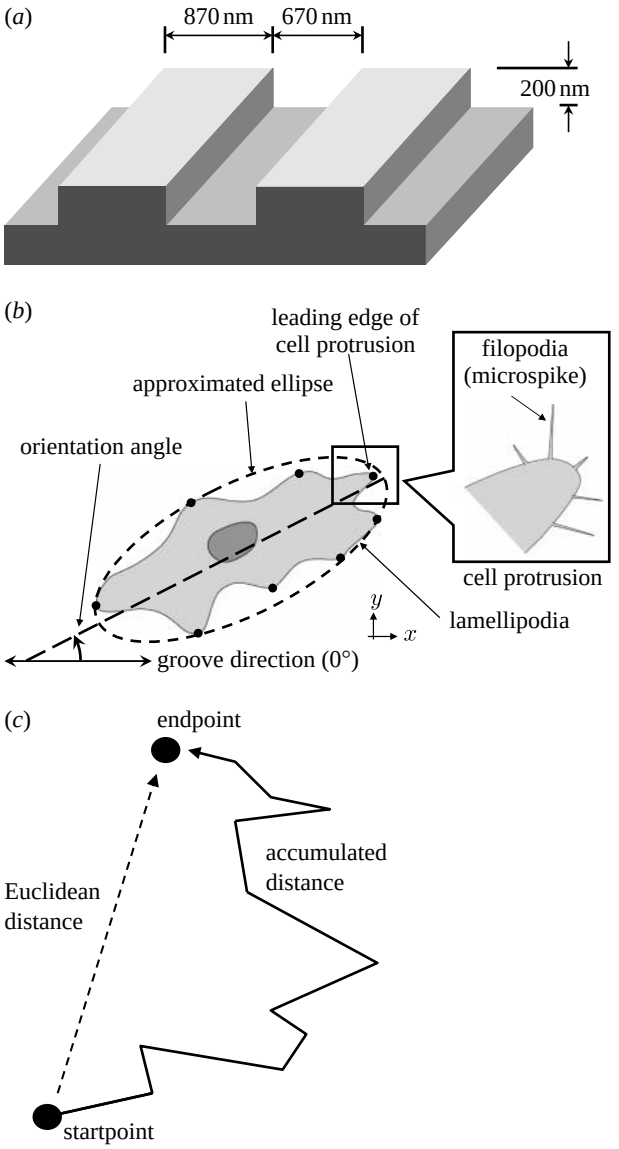

Scheme 1. (*a*) Dimensions of the NG pattern. (*b*) Terminologies used in this study. (*c*) Schematic of accumulated distance and Euclidean distance of movements of the leading edge of the cell protrusion.

2.4. Quantification of orientation angle

Cell orientation angles were quantified by the analysis of immunostained images or low-magnification time-lapse phase contrast images using ImageJ. The orientation angle of an

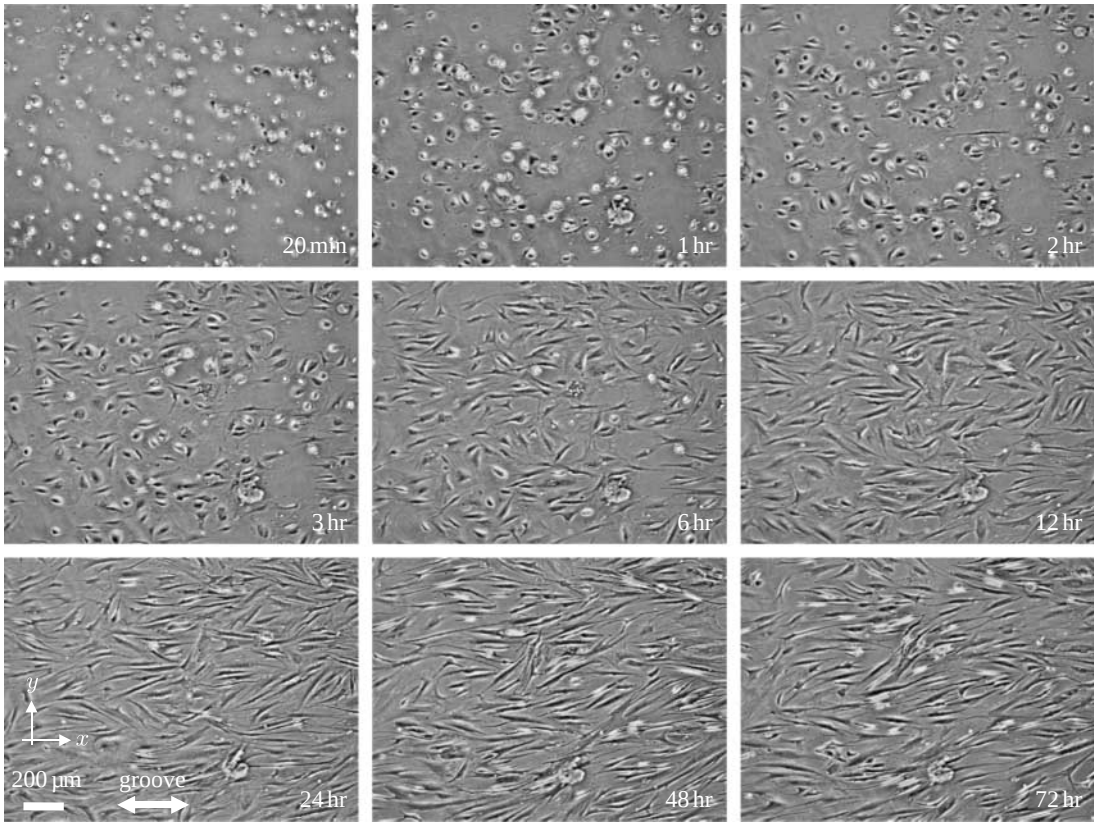

Figure 1. Low-magnification time-lapse images of MSCs seeded on the NG pattern. The NG lines were parallel to the x-axis. Recording under the time-lapse microscope started from 20 min post-seeding. Scale bar, 200 μm. See also the electronic supplementary material, movie 1.

individual cell was determined as the angle between the groove direction and the direction of the longer axis of the approximated ellipse, which approximates to the cell shape (scheme 1*b*). The distribution of cell orientation was estimated by a wrapped normal distribution, as previously reported (Dakin *et al.* 2005; Bashur *et al.* 2006; Agostinelli 2007). Briefly, the probability distribution function was adapted from Fisher (1993) for a periodicity of π radians as follows:

$$f(\theta) = \frac{1}{\pi}\left(1 + 2\sum_{p=1}^{\infty}\rho^{p^2}\cos(2p(\theta-\pi))\right), \tag{2.1}$$

$$\rho = \frac{1}{n}\sqrt{\left(\sum_{i=1}^{n}\cos 2\theta_i\right)^2 + \left(\sum_{i=1}^{n}\sin 2\theta_i\right)^2}, \tag{2.2}$$

and

$$\mu = \tan^{-1}\left(\frac{\sum_{i=1}^{n}\sin 2\theta_i}{\sum_{i=1}^{n}\cos 2\theta_i}\right), \tag{2.3}$$

where ρ is the mean resultant length and μ is the mean angle. These parameters were determined from a set of n measured cell orientation angles, θ_i. The angular standard deviation (s.d.), σ, for the distribution was determined by the following equation:

$$\sigma = \frac{1}{2}\sqrt{-2\ln\rho}. \tag{2.4}$$

2.5. Tracking of cell protrusions

The leading edges of cell protrusions were tracked through all of the captured images using the MTrackJ plug-in (v. 1.2.0) and Chemotaxis and Migration Tool plug-in (v. 1.01, distributed by ibidi GmbH, München, Germany) for ImageJ. The position of each leading edge was plotted in the coordinate axis, where the origin was the position where each edge first appeared and the x-axis was parallel to the grooves (scheme 1*b*). Tracking was terminated when the tip of the cell protrusion disappeared or recording ended. The distribution of protrusions was quantitatively compared by the s.d. of the angle between the vector of the endpoint of cell protrusion and x-axis calculated from equation (2.4). From the start point to the endpoint of each leading edge, an accumulated distance and the Euclidean distance were calculated as defined in scheme 1*c*. The velocity of a leading edge of a cell protrusion was defined as an accumulated distance of each edge divided by time (scheme 1*c*). The directionality of a leading edge of a cell protrusion was defined as given in the following equation:

$$\text{directonality} = \frac{\text{Euclidean distance}}{\text{accumulated distance}}. \tag{2.5}$$

2.6. Immunostaining

Cells were stained with F-actin and vinculin. Cultures were fixed with 4 per cent paraformaldehyde (Nacalai Tesque, Inc., Kyoto, Japan) for 15 min, permeabilized with 0.2 per cent Triton-X (Wako) for 3 min, blocked with 2 per cent skimmed milk (Nacalai) for 1 hour at room temperature and incubated with anti-mouse vinculin (Chemicon, CA, USA) (1 : 200 dilution) overnight at 4°C. Then, they were washed with 0.05 per cent polyoxyethylene sorbitan monolaurate (Tween 20, Wako, Osaka, Japan) for 15 min thrice at room temperature and treated with Alexa-594-conjugated phalloidin (Invitrogen) (1 : 40 dilution) for F-actin staining, Hoechst

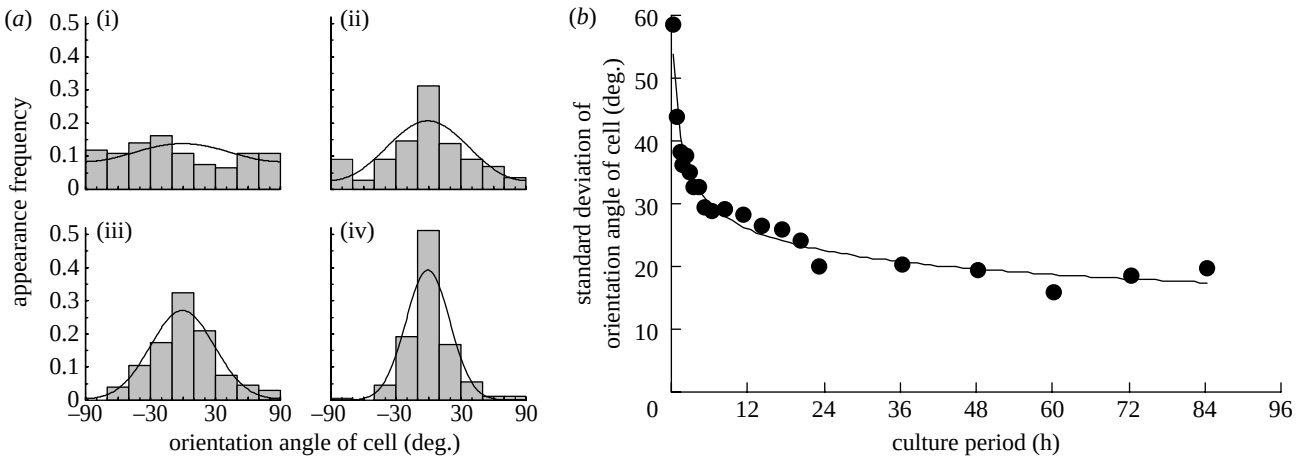

Figure 2. Cell orientation angle against the NG lines and the angular s.d. (*a*) Histograms of cell orientation angle against NG lines at (i) 20 min (s.d. = 58.4), (ii) 1 hour (s.d. = 38.1), (iii) 6 hours (s.d. = 28.9) and (iv) 24 hours (s.d. = 19.4) post-seeding. Each figure includes the angular s.d. calculated from the wrapped normal distribution (see equation (2.4) in the text). (*b*) Time course of the angular s.d.

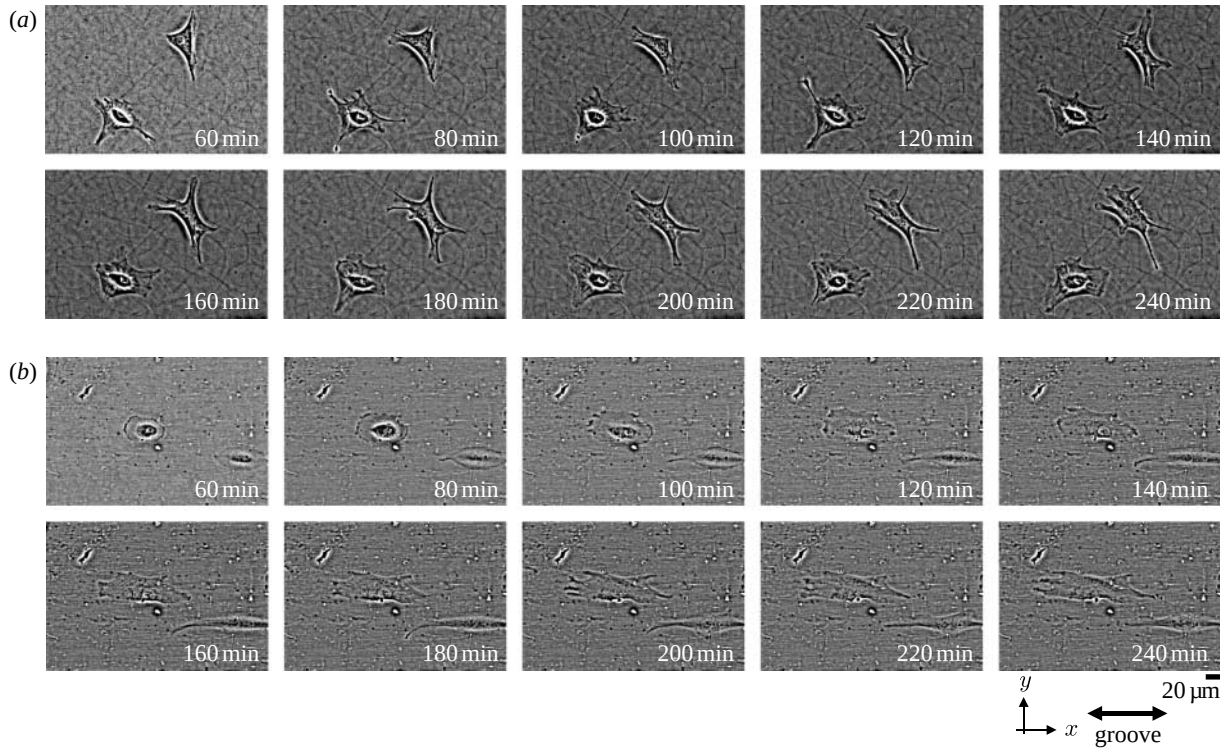

Figure 3. Comparison of time-lapse images of MSCs seeded on (*a*) a non-treated (NT) flat substrate and (*b*) an NG substrate. Cultures were incubated for 60 min after cell seeding at 37°C, 5% CO_2 and followed by recording under a time-lapse microscope every 2.5 min. Images of every 20 min are shown. In NG images, the NG lines were parallel to the x-axis. Scale bar, 20 μm. See also the electronic supplementary material, movies 2 and 3.

33342 (Dojindo, Kumamoto, Japan) (1 : 1000 dilution) for nucleus staining and Alexa-488-conjugated mouse anti-IgG (Invitrogen) (1 : 500 dilution) for vinculin staining, for 30 min at room temperature. Stained cultures were mounted on slides with a light anti-fade reagent (Vectashield, Vector Laboratories, Burlingame, CA, USA) and observed using a fluorescence inverted microscope (IX71, Olympus, Tokyo, Japan).

2.7. Statistical analysis

Comparisons between two groups were made using Student's t-tests. $p < 0.05$ was considered statistically significant. All statistical calculations were performed using the software JMP v. 5.1.1.

3. RESULTS

3.1. Cell alignment

In a previous study, we observed contact guidance of MSC alignment on NG substrates when the NG depth was more than 90 nm (Fujita *et al.* 2008). In this study, NG plates with 200 nm groove depth, 870 nm ridge width and 670 nm groove width were employed (scheme 1*a* and the electronic supplementary material,

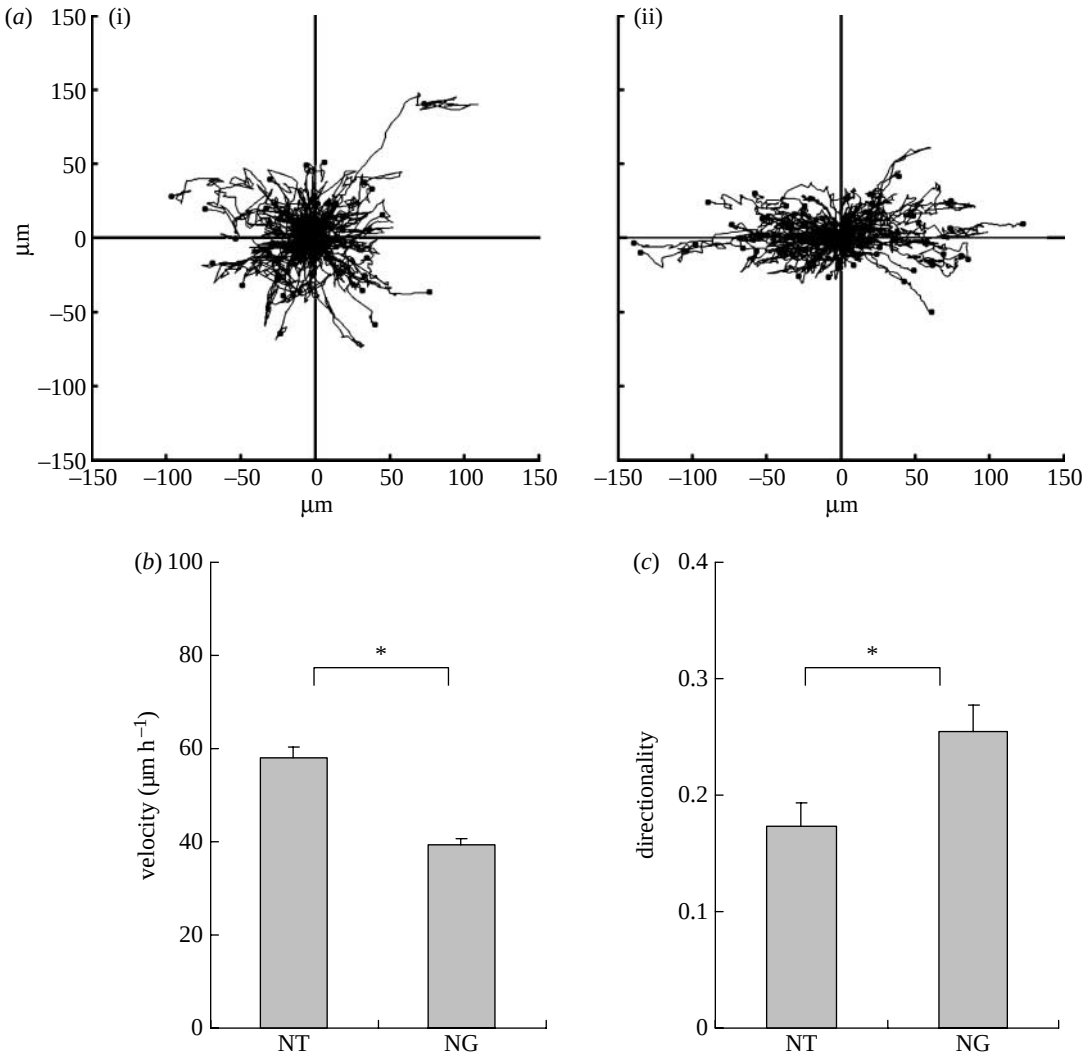

Figure 4. Movements of leading edges of cell protrusions. (*a*) Tracks of leading edges of protrusions of cells on (i) NT flat substrate (number of tracks = 62; s.d. = 81.5) and (ii) the NG substrate (number of tracks = 80; s.d. = 32.5). Start point of a leading edge of each cell protrusion was set at the origin of the coordinate axes, its location every 2.5 min was plotted and a filled circle indicates its endpoint after observation. The values inserted represent the s.d. of angles between the lines from the origin to filled circles and the x-axis. (*b*) Average velocity of leading edges. The velocity of each leading edge was determined by dividing the contour length by observed time. Values were given as mean $\pm$s.d. for $n = 62$ protrusions for the flat substrate and 80 for the NG substrate, of 10 randomly selected cells, respectively. (*c*) Directionality of leading edge movement, which was defined as the ratio of the Euclidean distance and accumulated distance. Asterisks represent a significant difference ($p < 0.05$) between two groups.

figure 1*a*). Dynamic cell behaviours on the NG plate were observed using time-lapse microscopes. Cells on the NG plate started to align along the NG patterns just after cell seeding, as shown in figure 1, and the dynamic features of this alignment can also be viewed in the electronic supplementary material, movie 1. Cells extended in parallel with the NG pattern and aligned with each other during the subsequent 24 hours of culture. Cell alignment was maintained for at least 4 days following this period.

To express cell alignment quantitatively, we determined the orientation angles of individual cells ($n > 140$ for each time point) against the groove direction (scheme 1*b*), and calculated the s.d., σ, of the distribution of the orientation angles at each time point using equation (2.4). No specific orientation of cells in a specific direction was observed at 20 min after cell seeding, as shown in figure 1. Figure 2*a* shows cell orientation more quantitatively by histograms and the angular s.d. (σ). It was $\sigma = 58.4$ at 20 min. After 1 hour of culture, a clear peak at 0° was observed in the histogram of the orientation angle distribution. This tendency became much clearer and the angular s.d. decreased rapidly with time afterwards. Figure 2*b* shows the time course of the values of the s.d., σ. The s.d. value sharply decreased with time during the initial several hours and remained at approximately 20 afterwards, indicating maintenance of cell alignment along the grooves.

3.2. Cell protrusions

To elucidate the mechanism of cell morphological changes, we focused attention on cell protrusions (scheme 1*a*). A cell protrusion is defined as a thicker protrusive structure in amoeboid cells, carrying

lamellipodia, pseudopodia, filopodia (microspikes) and microvilli (Adams 2002; DeMali & Burridge 2003). Figure 3*a* and the electronic supplementary material, movie 2, show that cells extended their cell protrusions in all directions on a flat substrate. Lifetimes of the cell protrusions differed from one another, but no clear dependence of lifetime on direction was seen on the flat substrate. Figure 3*b* and the electronic supplementary material, movie 3, however, show that cells extended cell protrusions in all directions equally on the NG plate, as seen on the flat substrate, but cell protrusions that extended in the groove direction remained longer than those that were perpendicular to the groove direction. Consequently, cells elongated and aligned along the groove direction.

To evaluate the extension length and the direction of cell protrusions more quantitatively, the leading edges of the cell protrusions were tracked every 2.5 min from 1 to 7 hours after cell seeding. Movements of the cell protrusions from the cells shown in figure 3*a*,*b* are presented in the electronic supplementary material, movies 2 and 3. The trajectories of the leading edges of cell protrusions are plotted in figure 4*a*. The s.d. of the angles of the cell protrusions against the groove direction were 32.5 on the NG plate but 81.5 on the flat plate. Thus, the leading edges of the cell protrusions extended along the grooves on the NG plate. Additionally, the numbers of protrusion appearances per cell in an hour were 1.17 ± 0.37 for cells on the NG and 0.98 ± 0.25 for cells on the flat plate. No significant difference was observed between these. On the other hand, their lifespans (i.e. time from appearance to retraction) were 265 ± 91 and 154 ± 50 min for the cells on the NG and on the flat plates, respectively. Protrusions existed longer on the NG plate than the flat plate. These results indicate that cells tend to elongate along the NG patterns, although cell protrusions emerge at the same frequency.

The averaged velocities and the directionality of edge movement of cell protrusions were determined as described in §2. Significant differences were observed in the velocities and the directions of movements of cell protrusions between cells cultured on non-treated (NT) plates and NG plates, as shown in figure 4*b*,*c*. Moreover, directionality was higher on the NG plate than on the NT plate. This outcome implies that the movement of the edge of cell protrusions on the NG plate would confine the movements of cell protrusions along the grooves because higher directionality indicates linear movement of cell protrusions.

3.3. Focal adhesion points

To give some insights into the anisotropic movements of cell protrusions, focal adhesion points under a cell protrusion onto the NG pattern were examined in detail by immunohistochemical staining of actin filaments and vinculin found at focal adhesion points (figure 5 and the electronic supplementary material, figure 2). Vinculin was found only on the ridges of the NG pitches as seen for vinculin staining in figure 5. When the cell protrusions extended parallel to the groove direction, vinculin aligned parallel to the NG direction and actin

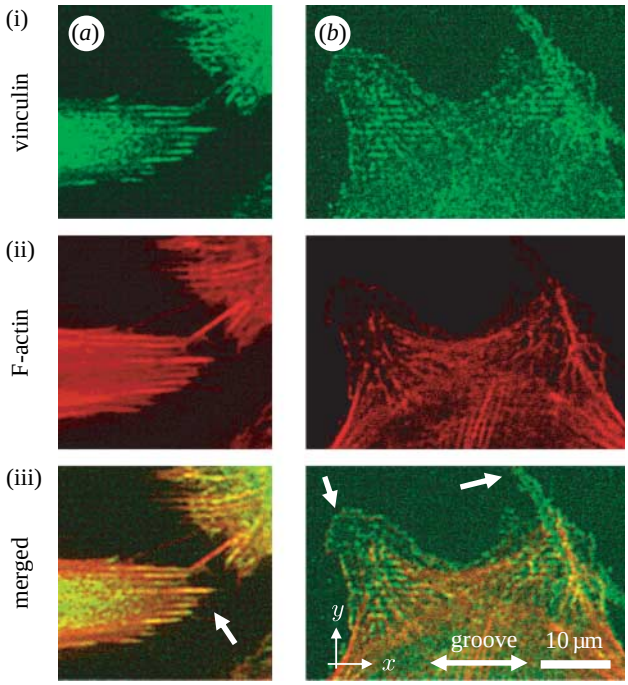

Figure 5. Immunohistochemical staining of vinculin and actin filaments of MSCs after 4 days of culture on the NG substrate. A cell protrusion extended (*a*) parallel and (*b*) perpendicular to the NG lines. (i) Vinculin was stained with Alexa-488-conjugated antibody (green) and (ii) F-actin of the cytoskeleton was stained with Alexa-594-conjugated phalloidin (red) and (iii) merged images are shown. Arrows indicate leading edges of cell protrusions. Scale bar, 10 µm.

filaments aligned parallel to vinculin and their terminations attached to vinculin as shown in figure 5*a*. A long area of focal adhesion is expected to be able to resist the contraction force generated by actin filaments. On the other hand, when cell protrusions extended perpendicular to the groove direction, vinculin aligned parallel to the NG direction, but fragmented, and actin filament terminations attached to vinculin, but were not following the vinculin lines and were not aligning to a specific direction as seen in figure 5*b* and the electronic supplementary material, figure 2, and illustrated in scheme 2*a*. The cell protrusions will be easily retracted owing to fragmented focal adhesion. These results suggest that the retraction phase of the cell protrusions plays a role in the formation of cell contact guidance. Biggs *et al.* (2008*a*,*b*) focused on adhesion points and found that nanotopography affected adhesion formation. Our results are consistent with their observations of fixed cells using a scanning electron microscope.

3.4. Filopodial probing

It has been reported that filopodia play a sensory or exploratory role when a cell migrates and extends (Faix & Rottner 2006). The diameters of filopodia are 250–400 nm (McClay 1999), smaller than the width of the ridge and the groove of our NG plate. Filopodia were expected to attach to the ridges and to reach the bottom of the grooves without difficulty. Filopodia movements were followed by a time-lapse microscope to visualize their role in cell alignment along the NG plate.

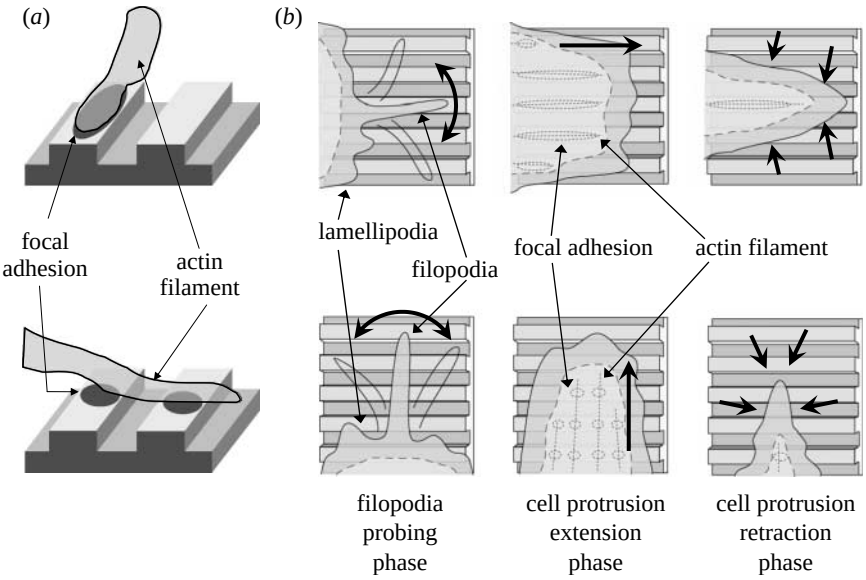

Scheme 2. Model for cell alignment on the NG substrate. (*a*) Actin filaments parallel to the grooves form wide focal adhesions at filament terminations. On the other hand, termination of perpendicular filaments is fragmented because focal adhesion is formed only on the ridge. (*b*) Filopodia movements are isotropic, i.e. no specific direction was observed for their extension and retraction against the NG structure. This finding suggests that filopodia probing does not play a major role in cell alignment. Cell protrusions isotropically extended, but some of them that were perpendicular to the NG pattern more rapidly retracted than those parallel to the NG pattern. These cell protrusion dynamics force a cell to elongate and align along the NG pattern.

A representative cell protrusion was observed under high magnification (80 × objective lens) on a time-lapse microscope to see the dynamic features of the filopodia. Figure 6*b* and the electronic supplementary material, movies 4 and 5, show the representative movements of filopodia. Filopodia indicated by arrows in the figure moved as if they were probing the surroundings of the cell protrusion. Then, some cell protrusions invaded the probed areas, as indicated by arrowheads. Cell protrusions that extended perpendicular to the NG direction retracted more rapidly than those parallel to the grooves (arrow, R), while, on a flat substrate, this repeated probing and retraction of the cell protrusion was rarely observed (electronic supplementary material, movie 6). In these two cases, however, no difference in filopodia movements was observed. These facts suggest that filopodia cannot distinguish topological differences or that filopodia can do so but that the retracting phase of cell protrusions is a major factor for cell alignment along the NG patterns.

4. DISCUSSION

A large number of studies have examined the effects of surface topography on cell behaviours or contact guidance. Dalby *et al.* (2004) reported that filopodia of human fibroblasts can sense topography down to a pitch of 35 nm in diameter and 50 nm in depth and that filopodial probing acts as an initial trigger for cell alignment in response to the topography of substrates. Teixeira *et al.* (2003) employed human corneal epithelial cells. In their study, they found that filopodia aligned along the grooves and that cells attached to the ridge and aligned along the NG pattern. From these findings, they speculated that filopodia sense differences in surface topography and induce cell alignment. In their other report, however, filopodia aligned perpendicular to the grooves (Teixeira *et al.* 2006). They mentioned that these two contradictory results reflected a difference in culture media. Wójciak-Stothard *et al.* (1996) reported that filopodia extending perpendicular to the groove direction were more frequently observed than those along the NG pattern, even though they were in cells that had aligned along the NG pattern. The role of filopodial probing remains controversial. Most researchers assessed this relationship of filopodial movements and cell alignments after cells were fixed with formaldehyde, methanol or glutaraldehyde.

We expected that the examination by time-lapse microscopes of the kinetics of cell alignment and dynamic features of cell protrusions and filopodia would give more detailed insights into cell responses to surface topography and the roles of cell protrusions and filopodia in contact guidance of cells. As shown in figure 6 and the electronic supplementary material, movie 6, filopodia moved as if they were probing the surroundings of the cell protrusion, and then some cell protrusions invaded the probed areas. Cell protrusions that extended perpendicular to the NG direction tended to retract more rapidly than those parallel to the grooves. From these facts, we think that the retracting phase of cell protrusions is a more important factor for cell alignment along the NG patterns (scheme 2) than filopodial sensing. On the other hand, it has been reported that filopodia can distinguish topological differences and cell protrusions follow filopodia movements, resulting in cell alignment (Teixeira *et al.* 2003, 2006; Dalby *et al.* 2004). At this point, it is difficult to identify which is the major mechanism in cell alignment on the NG pattern. We should carefully carry out additional experiments, such as the observation of the extension of filopodia under much shorter interval than this experiment, every 4 s, and clear visualization of filopodia movements employing fluorescent labelling.

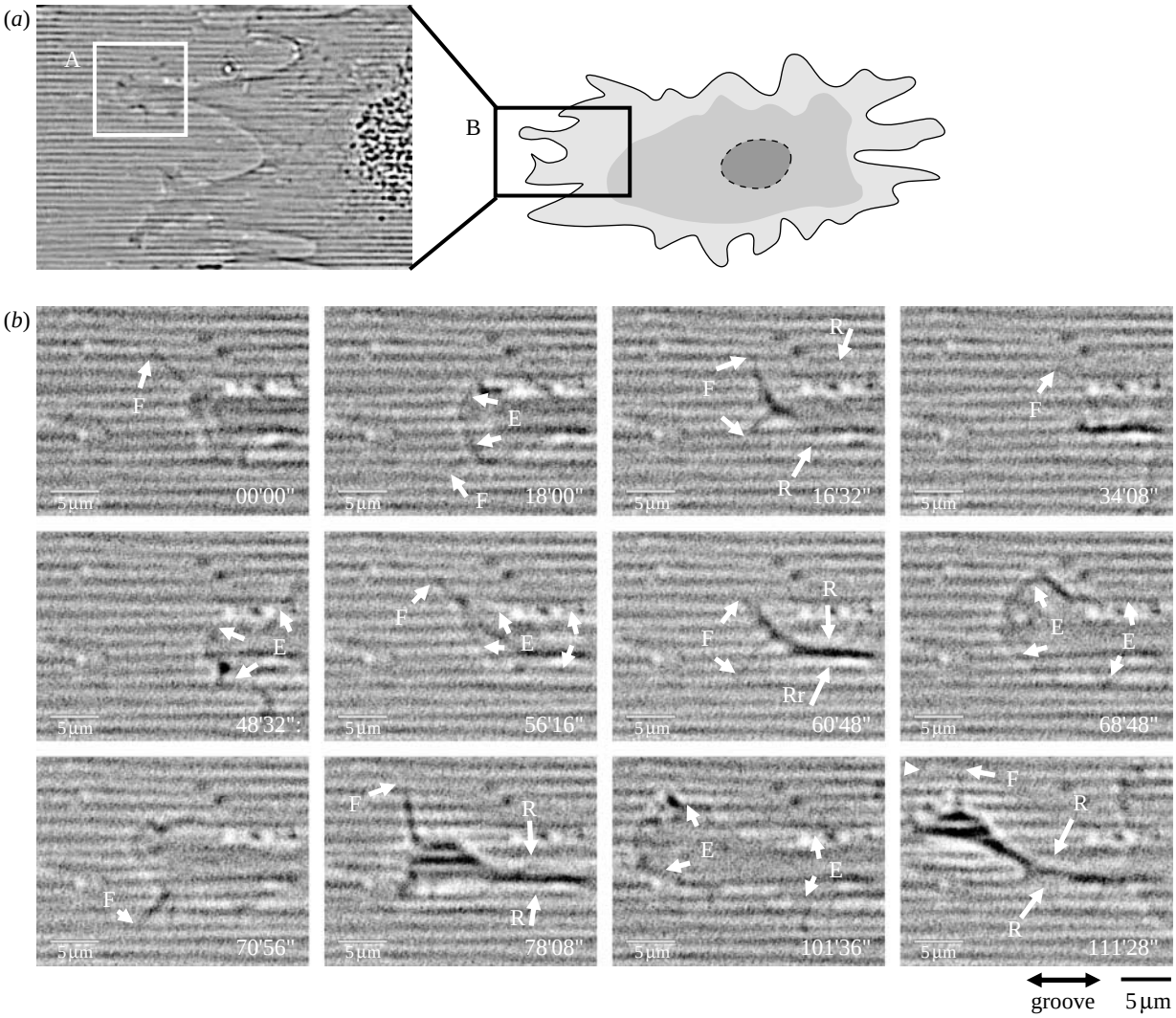

Figure 6. Observation of filopodia under high magnification. (*a*) Schematic of the observation area. Electronic supplementary material, movie 4, shows the rectangular area (A) and movie 5a shows the area (B). Pictures were captured with time-lapse microscopy every 4 s. (*b*) The extension and retraction of the leading edge of the cell protrusion and precession movements of representative filopodia on the NG substrate. Arrows in the figure indicate (F) filopodial probing, (E) extending cell protrusion and (R) retracting cell protrusion. Scale bar, 5 µm.

Cell protrusions extended around cells. Some of those perpendicular to the NG pattern tended to rapidly retract compared to those parallel to the NG pattern. As shown in figure 5, when cell protrusions extended parallel to NG lines, both vinculin and actin filaments also aligned parallel to the NG lines; but when cell protrusions extended perpendicular to the NG lines, vinculin staining was fragmented, and no clear alignment of actin filaments was observed. The latter focal adhesion—the fragmented vinculin expression area—is expected to be a weaker adhesion than the longer vinculin expression area, resulting in easy retract of cell protrusions perpendicular to the NG.

MSCs are multipotent stem cells that can differentiate into osteoblasts, adipocytes, chondrocytes and other kinds of mesenchymal cells (Pittenger *et al.* 1999). The morphology of MSCs can determine their fates, such as proliferation or differentiation direction (McBeath *et al.* 2004; Engler *et al.* 2006). As shown in figure 1, the morphology of MSCs is affected by the nanostructure of cell culture substrates. Thus, we expected that the differentiation direction of MSCs can be controlled by the substrate topography. In future studies, we will carefully examine the effect of NG patterns on MSC differentiation.

5. CONCLUSION

We observed living cells on an NG pattern using time-lapse microscopes to clearly demonstrate the dynamic features of cell alignment along the NG pattern. Cell protrusions perpendicular to the NG pattern retracted more rapidly than those parallel to it. The anisotropic retraction rate of cell protrusions would induce cell elongation and alignment along the NG pattern. Filopodial roles in cell alignment are controversial, and detailed dynamic observations are required to elucidate them in future.

This study was partly supported by the Knowledge-Based Cluster Creation Project, MEXT and Leading Project: Development of Artificial Organs Utilizing Nanotechnology and Materials Science.

REFERENCES

Adams, J. C. 2002 Regulation of protrusive and contractile cell-matrix contacts. *J. Cell Sci.* **115**, 257–265.

Agostinelli, C. 2007 Robust estimation for circular data. *Comput. Stat. Data Anal.* **51**, 5867–5875. (doi:10.1016/j.csda.2006.11.002)

Bashur, C. A., Dahlgren, L. A. & Goldstein, A. S. 2006 Effect of fiber diameter and orientation on fibroblast morphology and proliferation on electrospun poly(D,L-lactic-*co*-glycolic acid) meshes. *Biomaterials* **27**, 5681–5688. (doi:10.1016/j.biomaterials.2006.07.005)

Biggs, M. J., Richards, R. G., Wilkinson, C. D. & Dalby, M. J. 2008*a* Focal adhesion interactions with topographical structures: a novel method for immuno-SEM labelling of focal adhesions in S-phase cells. *J. Microsc.* **231**, 28–37. (doi:10.1111/j.1365-2818.2008.02013.x)

Biggs, M. J., Richards, R. G., McFarlane, S., Wilkinson, C. D., Oreffo, R. O. & Dalby, M. J. 2008*b* Adhesion formation of primary human osteoblasts and the functional response of mesenchymal stem cells to 330 nm deep microgrooves. *J. R. Soc. Interface* **5**, 1231–1242. (doi:10.1098/rsif.2008.0035)

Charest, J. L., García, A. J. & King, W. P. 2007 Myoblast alignment and differentiation on cell culture substrates with microscale topography and model chemistries. *Biomaterials* **28**, 2202–2210. (doi:10.1016/j.biomaterials.2007.01.020)

Clark, P., Connolly, P., Curtis, A. S. G., Dow, J. A. T. & Wilkinson, C. D. W. 1990 Topographical control of cell behaviour. II. Multiple grooved substrata. *Development* **108**, 635–644.

Curtis, A. & Wilkinson, C. 1997 Topographical control of cells. *Biomaterials* **18**, 1573–1583. (doi:10.1016/S0142-9612(97)00144-0)

Dakin, S. C., Mareschal, I. & Bex, P. J. 2005 Local and global limitations on direction integration assessed using equivalent noise analysis. *Vision Res.* **45**, 3027–3049. (doi:10.1016/j.visres.2005.07.037)

Dalby, M. J., Gadegaard, N., Riehle, M. O., Wilkinson, C. D. & Curtis, A. S. 2004 Investigating filopodia sensing using arrays of defined nano-pits down to 35 nm diameter in size. *Int. J. Biochem. Cell Biol.* **36**, 2005–2015. (doi:10.1016/j.biocel.2004.03.001)

Dalby, M. J., Gadegaard, N., Tare, R., Andar, A., Riehle, M. O., Herzyk, P., Wilkinson, C. D. & Oreffo, R. O. 2007 The control of human mesenchymal cell differentiation using nanoscale symmetry and disorder. *Nat. Mater.* **6**, 997–1003. (doi:10.1038/nmat2013)

Dalton, B. A., Walboomers, X. F., Dziegielewski, M., Evans, M. D. M., Taylor, S., Jansen, J. A. & Steele, J. G. 2001 Modulation of epithelial tissue and cell migration by microgrooves. *J. Biomed. Mater. Res.* **56**, 195–207. (doi:10.1002/1097-4636(200108)56:2<195::AID-JBM1084>3.0.CO;2-7)

DeMali, K. A. & Burridge, K. 2003 Coupling membrane protrusion and cell adhesion. *J. Cell Sci.* **116**, 2389–2397. (doi:10.1242/jcs.00605)

Diehl, K. A., Foley, J. D., Nealey, P. F. & Murphy, C. J. 2005 Nanoscale topography modulates corneal epithelial cell migration. *J. Biomed. Mater. Res. A* **75**, 603–611. (doi:10.1002/jbm.a.30467)

Engler, A. J., Sen, S., Sweeney, H. L. & Discher, D. E. 2006 Matrix elasticity directs stem cell lineage specification. *Cell* **126**, 677–689. (doi:10.1016/j.cell.2006.06.044)

Faix, J. & Rottner, K. 2006 The making of filopodia. *Curr. Opin. Cell Biol.* **18**, 18–25. (doi:10.1016/j.ceb.2005.11.002)

Fisher, N. I. 1993 *Statistical analysis of circular data*. New York, NY: Cambridge University Press.

Flemming, R. G., Murphy, C. J., Abrams, G. A., Goodman, S. L. & Nealey, P. F. 1999 Effects of synthetic micro- and nano-structured surfaces on cell behavior. *Biomaterials* **20**, 573–588. (doi:10.1016/S0142-9612(98)00209-9)

Fujita, S., Ono, D., Ohshima, M. & Iwata, H. 2008 Supercritical CO_2-assisted embossing for studying cell behaviour on microtextured surfaces. *Biomaterials* **29**, 4494–4500. (doi:10.1016/j.biomaterials.2008.08.027)

Keselowsky, B. G., Collard, D. M. & García, A. J. 2004 Surface chemistry modulates focal adhesion composition and signaling through changes in integrin binding. *Biomaterials* **25**, 5947–5954. (doi:10.1016/j.biomaterials.2004.01.062)

Kurpinski, K., Chu, J., Hashi, C. & Li, S. 2006 Anisotropic mechanosensing by mesenchymal stem cells. *Proc. Natl Acad. Sci. USA* **103**, 16 095–16 100. (doi:10.1073/pnas.0604182103)

Lim, J. Y. & Donahue, H. J. 2007 Cell sensing and response to micro- and nanostructured surfaces produced by chemical and topographic patterning. *Tissue Eng.* **13**, 1879–1891. (doi:10.1089/ten.2006.0154)

McBeath, R., Pirone, D. M., Nelson, C. M., Bhadriraju, K. & Chen, C. S. 2004 Cell shape, cytoskeletal tension, and RhoA regulate stem cell lineage commitment. *Dev. Cell* **6**, 483–495. (doi:10.1016/S1534-5807(04)00075-9)

McClay, D. R. 1999 The role of thin filopodia in motility and morphogenesis. *Exp. Cell Res.* **253**, 296–301. (doi:10.1006/excr.1999.4723)

Navarro, M., Aparicio, C., Charles-Harris, M., Ginebra, M. P., Engel, E. & Planell, J. A. 2006 Development of a biodegradable composite scaffold for bone tissue engineering: physicochemical, topographical, mechanical, degradation, and biological properties. *Adv. Polym. Sci.* **200**, 209–231. (doi:10.1007/12_068)

Park, J. S., Chu, J. S. F., Cheng, C., Chen, F., Chen, D. & Li, S. 2004 Differential effects of equiaxial and uniaxial strain on mesenchymal stem cells. *Biotechnol. Bioeng.* **88**, 359–368. (doi:10.1002/bit.20250)

Pittenger, M. F. *et al.* 1999 Multilineage potential of adult human mesenchymal stem cells. *Science* **284**, 143–147. (doi:10.1126/science.284.5411.143)

Su, W. T., Liao, Y. F. & Chu, I. M. 2007 Observation of fibroblast motility on a micro-grooved hydrophobic elastomer substrate with different geometric characteristics. *Micron* **38**, 278–285. (doi:10.1016/j.micron.2006.04.008)

Teixeira, A. I., Abrams, G. A., Bertics, P. J., Murphy, C. J. & Nealey, P. F. 2003 Epithelial contact guidance on well-defined micro- and nanostructured substrates. *J. Cell Sci.* **116**, 1881–1892. (doi:10.1242/jcs.00383)

Teixeira, A. I., McKie, G. A., Foley, J. D., Bertics, P. J., Nealey, P. F. & Murphy, C. J. 2006 The effect of environmental factors on the response of human corneal epithelial cells to nanoscale substrate topography. *Biomaterials* **27**, 3945–3954. (doi:10.1016/j.biomaterials.2006.01.044)

Witt, D., Klajn, R., Barski, P. & Grzybowski, B. A. 2004 Applications, properties and synthesis of ω-functionalized *n*-alkanethiols and disulfides—the building blocks of self-assembled monolayers. *Curr. Org. Chem.* **8**, 1763–1797. (doi:10.2174/1385272043369421)

Wójciak-Stothard, B., Curtis, A., Monaghan, W., MacDonald, K. & Wilkinson, C. 1996 Guidance and activation of murine macrophages by nanometric scale topography. *Exp. Cell Res.* **223**, 426–435. (doi:10.1006/excr.1996.0098)

Zhu, B., Lu, Q., Yin, J., Hu, J. & Wang, Z. 2005 Alignment of osteoblast-like cells and cell-produced collagen matrix induced by nanogrooves. *Tissue Eng.* **11**, 825–834. (doi:10.1089/ten.2005.11.825)